Stealth Surface Modification of Surface-Enhanced Raman Scattering Substrates for Sensitive and Accurate Detection in Protein Solutions

Fang Sun, Jean-Rene Ella-Menye, Daniel David Galvan, Tao Bai, Hsiang-Chieh Hung, Ying-Nien Chou, Peng Zhang, Shaoyi Jiang, and Qiuming Yu*

Department of Chemical Engineering, University of Washington, Seattle, Washington 98195, United States

ABSTRACT Reliable surface-enhanced Raman scattering (SERS) based biosensing in complex media is impeded by nonspecific protein adsorptions. Because of the near-field effect of SERS, it is challenging to modify SERS-active substrates using conventional nonfouling materials without introducing interference from their SERS signals. Herein, we report a stealth surface modification strategy for sensitive, specific and accurate detection of fructose in protein solutions using SERS by forming a mixed self-assembled monolayer (SAM). The SAM consists of a short zwitterionic thiol, *N*,*N*-dimethyl-cysteamine-carboxybetaine (CBT), and a fructose probe 4-mercaptophenylboronic acid (4-MPBA). The specifically designed and synthesized CBT not only resists protein fouling effectively, but also has very weak Raman activity compared to 4-MPBA. Thus, the CBT SAM provides a stealth surface modification to SERS-active substrates. The surface compositions of mixed SAMs were investigated using X-ray photoelectron spectroscopy (XPS) and SERS, and their nonfouling properties were studied with a surface plasmon resonance (SPR) biosensor. The mixed SAM with a surface composition of 94% CBT demonstrated a very low bovine serum albumin (BSA) adsorption (~3 ng/cm^2), and moreover, only the 4-MPBA signal appeared in the SERS spectrum. With the use of this surface-modified SERS-active substrate, quantification of fructose over clinically relevant concentrations (0.01−1 mM) was achieved. Partial least-squares regression (PLS) analysis showed that the detection sensitivity and accuracy were maintained for the measurements in 1 mg/mL BSA solutions. This stealth surface modification strategy provides a novel route to introduce nonfouling property to SERS-active substrates for SERS biosensing in complex media.

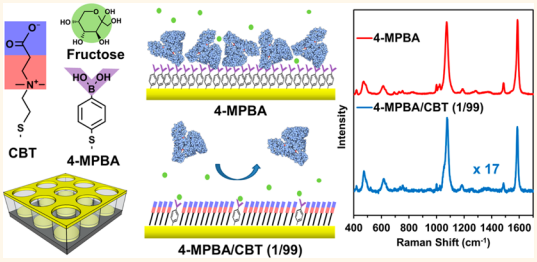

KEYWORDS: zwitterionic thiol · nonfouling · surface modification · complex media · surface-enhanced Raman scattering

Biosensing based on surface-enhanced Raman scattering (SERS) platforms has made tremendous progress due to the advances of controllable colloidal metallic nanoparticle synthesis, precise nanofabrication and surface modification techniques.[1−3] The extremely high sensitivity has been realized by well controlled metallic nanoparticle size, shape and distance, as well as different two-dimensional and three-dimensional plasmonic nanostructures.[4] The detection specificity can be obtained from the vibrational modes of the target molecule directly adsorbed on SERS-active substrate surfaces, or *via* Raman reporters and probes. The high sensitivity and molecular specificity of SERS have led to an enormous amount of biosensing applications, such as the detection of small biomolecules,[5,6] DNA strands,[7−9] proteins,[10] microorganisms,[11−13] and cancer cells.[14] Nevertheless, reliable biosensing based on SERS platforms in complex biological media is still challenging due to interfering species and nonspecific adsorption of proteins.[15] Background noise from interfering species could mask the signals from target analytes because a bare SERS-active surface lacks selectivity. Nonspecific adsorption of proteins could impede the adsorption of target analytes to SERS-active substrate surfaces.

To promote target analytes to SERS substrate surfaces and thus to reduce interferences, several surface modification methods have been developed. With the formation of mixed self-assembled monolayers (SAMs) of alkane or benzyl thiols on SERS-active substrates, small molecules such as glucose and

* Address correspondence to qyu@u.washington.edu.

Received for review November 11, 2014 and accepted March 4, 2015.

Published online March 04, 2015
10.1021/nn506447k

3,4-methylenedioxymethamphetamine (MDMA) partition to the mixed SAM layer, and thus enable the detections.[16,17] Instead of physical attractions, thiolated aptamers have been used to modify SERS substrates to recognize and bind analytes.[18,19] Then, the SERS detection was accomplished by measuring either the SERS signals of the Raman label conjugated to the analyte vasopressin[18] or the SERS signals of the analyte ricin.[19] Recognition between antibody−antigen has also been employed for SERS biosensing.[20,21] In these studies, molecules with thiolated phenyl ring or dithiolated multiple phenyl rings were used as probes or reporters to detect the antigens. In fact, surface modifications based on molecules of benzenethiol with different functional groups, which serve as probe molecules, have attracted more attention recently.[22−25] They can form SAMs on SERS-active substrates, creating strong and reproducible SERS signals. Density functional theory (DFT) calculations showed that the probes with benzenethiol structure on SERS-active substrates exhibit a large intrinsic Raman activity due to the chemical enhancement mechanism.[26] This offers a great advantage since the detection of analytes is achieved by monitoring the SERS spectral changes of the probe molecules upon interactions with targeted analytes. The strong SERS signals of phenyl rings can amplify the detection signals over other interferences. For example, 4-mercaptobenzoic acid (4-MBA) was used to functionalize gold or silver nanoparticles for intracellular pH sensing because the SERS spectrum of 4-MBA changes in response to the interaction between the carboxyl group and protons.[22,23] A specially designed peptide receptor conjugated with thiophenol group was modified on silver nanoparticles; quantitative detection of an oncogenic protein in cell extracts was accomplished by monitoring the SERS spectral changes due to the reorientation of the phenyl ring.[24] Our group recently reported the using of 4-mercaptophenylboronic acid (4-MPBA) for quantitative and selective detection of fructose in artificial urine also based on observing the relative SERS intensity changes of the totally and nontotally symmetric ring vibrational modes due to the symmetry breaking upon fructose binding to the boronic acid group.[25]

Despite the successful detections using these surface modifications, a suppression of sensitivity and accuracy in complex media was observed in comparison to the results obtained in simple buffer solutions.[24,25,27] It was found that nonspecific adsorbed proteins from the complex media formed a dense layer prohibiting the diffusion and recognition of target molecules. Thus, a nonfouling modification with high surface coverage is desired to resist the nonspecific protein adsorption in order to maintain the detecting sensitivity and accuracy, as well as to prolong the stability and lifetime of the SERS-active substrates. However, SERS is a near-field effect and is most sensitive to the first monolayer of molecules on the SERS-active substrate surfaces.[28] If the SERS-active substrate surface is occupied by the nonfouling modification, signals of the modification may dominate the spectrum as an overwhelming background that could cover or overlap with the signals from target molecules. Therefore, surface modification of SERS-active substrates pose a great challenge to produce the capabilities to resist fouling without introducing unwanted signals, and also can respond to the interactions of immobilized probe molecules to target molecules for sensitive, specific and accurate SERS detection in complex media.

To tackle this challenge, we developed a stealth surface modification approach by modifying SERS-active substrate surfaces with a mixed SAM, containing molecules with dramatically different intrinsic Raman activities. Selective detection and signal amplification are achieved by the molecule with strong Raman activity, while nonfouling properties are achieved by the molecule with weak Raman activity. In this work, we designed and synthesized a short zwitterionic thiol, *N*,*N*-dimethyl-cysteamine-carboxybetaine (CBT), and used it to modify SERS-active substrate surfaces. This modification provided the surface with nonfouling properties because the carboxybetaine headgroup can bind water strongly and resist protein adsorption.[29,30] CBT is expected to have a remarkably small Raman cross section as a small aliphatic molecule.[31] As a proof of concept, we formed 4-MPBA and CBT mixed SAMs on gold quasi-three-dimensional plasmonic nanostructure arrays (Q3D-PNAs)[11,25] to detect fructose in protein solutions as illustrated in Figure 1a. The surface composition of two components is critical for maximizing the nonfouling properties without reducing the sensitivity, specificity and accuracy of SERS sensing. Therefore, the mixed SAMs with different compositions were studied using SERS and X-ray photoelectron spectroscopy (XPS). Their nonfouling performances were assessed by a surface plasmon resonance (SPR) biosensor. An optimized ratio of CBT to 4-MPBA was determined and used to modify the Q3D-PNAs. Detections of fructose with the concentrations in the clinically relevant range were conducted in PBS buffers and BSA solutions. Partial least-squares regression (PLS) analysis was applied and the results showed that the sensitivity and accuracy were maintained for the detections in BSA solutions. The resistance to protein adsorption and the invisibility of its own SERS signal make CBT a viable option for the stealth surface modification of SERS-active substrates.

RESTULT AND DISCUSSION

SERS Spectra of Pure and Mixed SAMs. The short zwitterionic thiol, CBT, was designed to have a carboxybetaine headgroup, in which both cationic and anionic groups are on the same molecule. Due to the electrostatically induced hydration, it can be highly resistant to

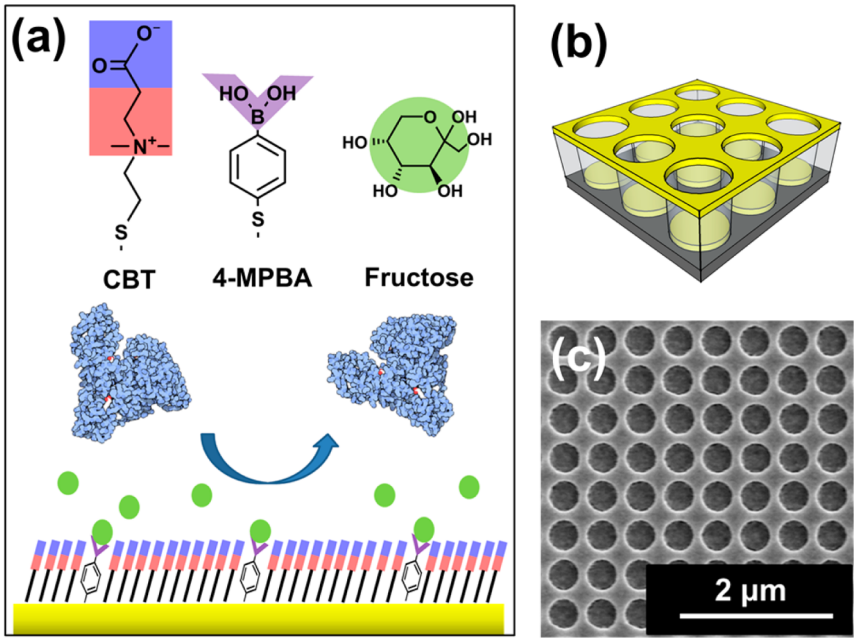

Figure 1. (a) Schematic illustration of mixed SAM of 4-MPBA and CBT on a gold Q3D-PNA SERS-active surface for fructose detection with the presence of proteins. (b) A 3D illustration of the Q3D-PNA composed of a separated gold thin film with nanoholes on top and gold nanodisks at the bottom of wells. (c) The top-view SEM image of a Q3D-PNA showing the diameter of ~400 nm.

nonspecific protein adsorption. There is a short spacer between the thiol and carboxybetaine group so that CBT and 4-MPBA can form a mixed SAM with similar height. The reaction route for the synthesis of CBT is presented in Scheme 1.

The pure CBT SAM was formed on the gold surface of a Q3D-PNA SERS substrate. The SERS spectrum of the CBT SAM in PBS is shown in Figure 2 (bottom purple line). Because of the small Raman scattering cross section, the measurement was achieved by collecting the spectrum with 10 accumulations to improve the signal-to-noise ratio. Characteristic peaks are observed from both the quaternary amine and carboxyl acid groups of CBT. The strong peaks at 756 and 1079 cm^{-1} are attributed to the symmetric and antisymmetric stretching vibration of the quaternary amine group (C_4N^+), respectively.[32,33] The stretching modes of the carboxyl acid group (COO^-) are illustrated at 1360 and 1585 cm^{-1}.[32,34] In addition, the CS stretching mode at 672 cm^{-1} and the in-plane bending mode of CS-Au at 847 cm^{-1} indicate that CBT adsorbs dissociatively as thiolate and forms a gold−sulfur bond.[35] The assignments of each peak are given in Table S1 in the Supporting Information.

Since CBT will serve as the nonfouling background while 4-MPBA will be used as a fructose reporter, the ratio of 4-MPBA to CBT of the mixed SAM is crucial in order to maximize the detection sensitivity while minimizing protein fouling. We modified the Q3D-PNA SERS substrates with 4-MPBA/CBT mixed SAMs using the molar ratios of 10/90 and 1/99 for 4-MPBA/CBT in bulk solutions. Figure 2 shows the SERS spectra of these two mixed 4-MPBA/CBT SAMs in PBS on Q3D-PNA SERS substrates. For comparison, the SERS spectra of the pure 4-MPBA SAM and pure CBT SAM are also shown in Figure 2. The SERS spectrum of pure 4-MPBA SAM is the same as we reported before.[25] The signal of a pure CBT SAM is about 170-fold lower than that of a pure 4-MPBA SAM. 4-MPBA has a larger Raman cross section than CBT from the benzene ring. In addition, thiolated linkers with conjugated π-electrons such as 4-MPBA allow more efficient electron transfer and molecular orbital overlapping, inducing a higher chemical enhancement factor over alkanethiols such as CBT.[36] The sharp difference between their intrinsic SERS activity ensures the possibility to increase the ratio of CBT in the 4-MPBA/CBT mixed SAM to provide a nonfouling modification while the SERS signals of CBT are still invisible. Indeed, as can be seen in Figure 2, the enlarged spectra of two mixed SAMs are very similar to those of the pure 4-MPBA SAM. The absolute intensities of characteristic peaks of 4-MPBA are decreased with a decreasing molar ratio of 4-MPBA to CBT in the bulk solution. No peaks of CBT are observed even in the enlarged spectrum of the mixed 4-MPBA/CBT (1/99) SAM. We noticed that ,with an increase in the ratio of CBT to 4-MPBA, the relative intensity ratio of the shoulder at 1065 cm^{-1} and the peak at 1075 cm^{-1} is increased, while that of the shoulder at 1574 cm^{-1} and the peak at 1587 cm^{-1} is decreased. This indicates a possible ring reorientation of 4-MPBA with the incorporation of CBT.

It is known that the ratio of two components forming a SAM on a surface is different from that in

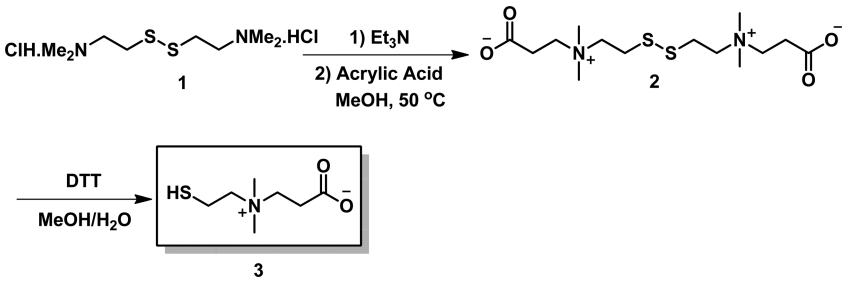

Scheme 1. Synthesis route of *N,N*-dimethyl-cysteamine-carboxybetaine (CBT).

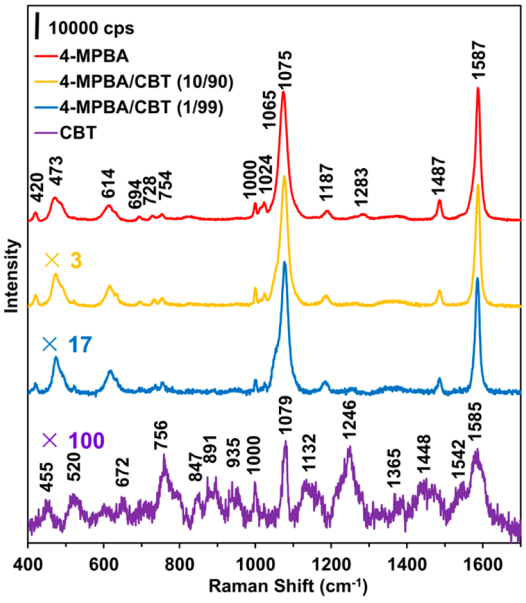

Figure 2. SERS spectra of pure 4-MPBA, 4-MPBA/CBT mixed SAMs and pure CBT on Q3D-PNAs in PBS. The mixed SAMs were formed with molar ratios 10/90 and 1/99 for 4-MPBA/CBT bulk solutions. The λ_{ex} = 785 nm, P_{laser} = 1 mW, and t = 10 s.

the bulk solution. We estimated the surface ratio of 4-MPBA/CBT by taking the ratio of the absolute intensity of the peak at 1075 cm^{-1}. We assumed that the surface coverage of pure 4-MPBA and 4-MPBA/CBT mixed SAMs is the same and that one CBT molecule replaces one 4-MPBA molecule on the SERS substrate surface. In this way, the decrease of the intensity of peak at 1075 cm^{-1} is directly due to the reducing number of 4-MPBA molecules on the surface. On the basis of this assumption, we obtained the surface ratios of 4-MPBA/CBT of mixed SAMs are 31/69 and 6/94 corresponding to the molar ratio of 10/90 and 1/99 in the bulk solutions, respectively. The higher fraction of 4-MPBA molecules in the SAMs may be attributed to the stronger $\pi-\pi$ interactions between phenol rings which make 4-MPBA SAMs more stable than the SAMs formed by the short alkanethiol.[37]

XPS Investigation of Pure and Mixed SAMs. The pure CBT SAM, pure 4-MPBA SAM and 4-MPBA/CBT mixed SAMs were further characterized using the surface sensitive technique XPS. Figure 3 shows the XPS high-resolution spectra of carbon (C 1s) and the detailed spectra of boron (B 1s) and nitrogen (N 1s) of the SAMs. The C 1s spectrum of the pure CBT SAM has two major peaks centered at 285.5 and 289.1 eV, corresponding to the carbon atom bonded to a nitrogen atom (C—N) or another carbon atom (C—C) and the carbon atom in the carboxylate group (O—C═O), respectively.[38] A small peak at 286.8 eV corresponding to the electron-deficient carbon atom bonded to a sulfur atom (C—S) was also fitted to the C 1s spectrum. The N 1s spectrum of the pure CBT SAM shows a peak at the binding energy of 402.3 eV.[38] The high-resolution spectrum of S 2p of the pure CBT SAM shown in Figure S1 in the Supporting Information can be fitted to one state of sulfur species at the surface with an S $2p_{3/2}$ binding energy at 162.0 eV, indicating sulfur atoms are bound to the surface. The C 1s, N 1s and S 2p spectra show that a well-packed monolayer of CBT is formed on the gold surface. The C 1s photoelectron peak of the pure 4-MPBA SAM is centered at 284.2 eV with a very small shoulder at 286.8 eV, corresponding to the carbon atoms of the aromatic ring (C═C) and the carbon atom bonded to sulfur atom (C—S), respectively, which are consistent with the spectrum reported before.[39] The B 1s spectrum of the pure 4-MPBA shows a peak at the binding energy of 191.2 eV. The high resolution C 1s spectra of the two 4-MPBA/CBT (10/90 and 1/99) mixed SAMs exhibit the characteristic peaks of both 4-MPBA and CBT but the intensities vary with the ratio of two components. The characteristic peak of the 4-MPBA SAM at ~284.2 eV decreases significantly to a tiny shoulder for the 4-MPBA/CBT (1/99) mixed SAM. The XPS detail spectra of B 1s and N 1s also show the same trend with the ratio of two components. There is almost no detectable B 1s peak but a strong N 1s peak for the 4-MPBA/CBT (1/99) mixed SAM. The XPS results clearly show that CBT occupies most of the surface for the 4-MPBA/CBT (1/99) mixed SAM. We calculated the ratio of the two components on the surface using the high resolution C 1s spectrum with the C═C peak for 4-MPBA and the/C—N and C—C peaks for CBT. The area ratio of the C═C peak to the he C—N and C—C peaks is 5/95, which is in a good agreement with the estimation from the SERS spectrum.

Nonfouling Evaluation of Mixed 4-MPBA/CBT SAMs. The nonspecific protein adsorption on different SAM modified gold surfaces was measured using an SPR

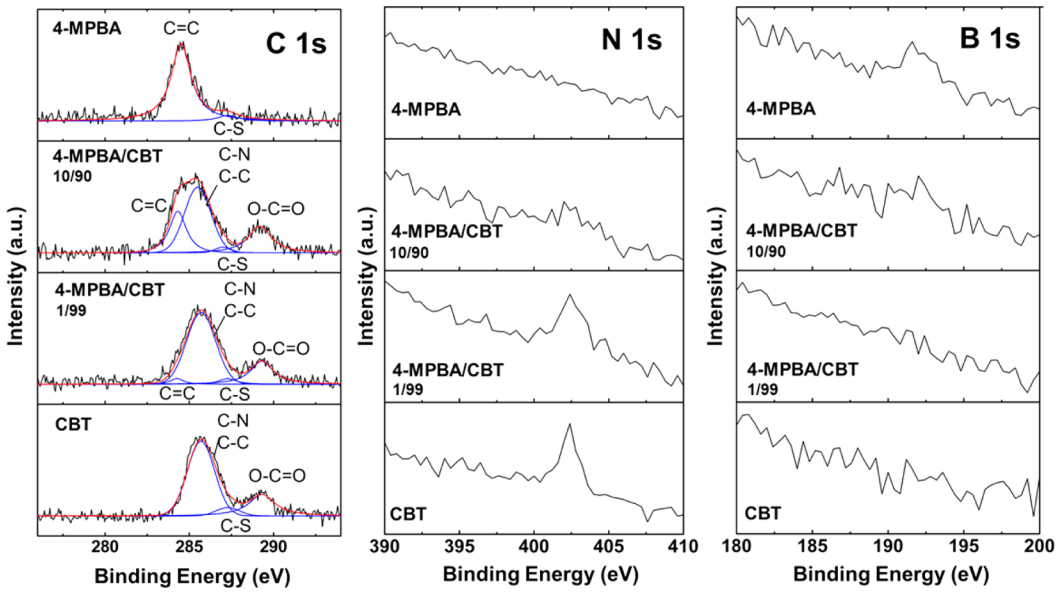

Figure 3. XPS high-resolution C 1s, detailed N 1s and B 1s spectra of pure 4-MPBA SAM, 4-MPBA/CBT (10/90 and 1/99) mixed SAMs and pure CBT SAM formed on gold surfaces.

biosensor. The pure CBT, pure 4-MPBA and 4-MPBA/CBT mixed SAMs were tested with a single protein—bovine serum albumin (BSA) solution (1 mg/mL) because BSA has been commonly used to block surfaces due to its high affinity to many surfaces. The typical SPR sensorgrams are shown in Figure 4. The pure CBT SAM shows a nonfouling property with the BSA adsorption of 2.2 ± 0.8 ng/cm^2. In contrast, the pure 4-MPBA SAM exibits a strong BSA adsorption of 148.4 ± 16.5 ng/cm^2. For the 4-MPBA/CBT mixed SAMs, Figure 4 shows that the mixed SAM formed by the ratio of 4-MPBA/CBT of 10/90 in the bulk solution can significantly reduce the BSA adsorption to 27.1 ± 8.8 ng/cm^2. With further increasing CBT in 4-MPBA/CBT mixed SAM to 1/99, the BSA adsorption is reduced to 3.0 ± 0.6 ng/cm^2, which is similar to the amount on the surface of the pure CBT SAM. Therefore, the 4-MPBA/CBT (1/99) mixed SAM is sufficient enough to resist protein adsorption, which was selected for the investigation of detecting fructose in protein solutions.

4-MPBA/CBT Mixed SAM Modified SERS-Active Substrates for Fructose Detection. As shown in Figure 2, although the absolute SERS intensities of 4-MPBA in 4-MPBA/CBT mixed SAMs are decreased with the increasing of CBT ratio, the spectra are still dominated by the 4-MPBA signal. In our previous study, we demonstrated that the pure 4-MPBA SAM modified Q3D-PNA SERS substrate can sensitively and specifically detect fructose in artificial urine.[25] The symmetry breaking of 4-MPBA upon fructose binding leads to the change of area ratio between totally symmetric 8a ring mode (1574 cm^{-1}) and nontotally symmetric 8b ring mode (1587 cm^{-1}), which enables the detection. In this work, we first tested how the SERS signals of 4-MPBA change upon the binding of fructose to the 4-MPBA/CBT (1/99)

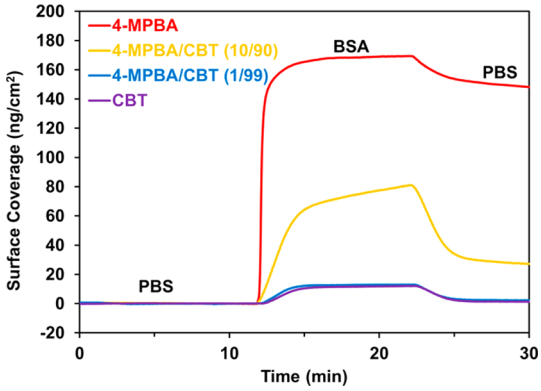

Figure 4. Typical SPR sensorgram of pure 4-MPBA SAM, 4-MPBA/CBT (10/90 and 1/99) mixed SAMs and pure CBT SAM on gold surfaces when exposed to 1 mg/mL bovine serum albumin (BSA) solution.

mixed SAM modified Q3D-PNA SERS substrate. We immersed a 4-MPBA/CBT (1/99) mixed SAM modified Q3D-PNA SERS substrate in 1 mM fructose PBS solution for 1 h to ensure binding equilibrium and then took the SERS spectrum. Figure 5 shows the SERS spectrum of 4-MPBA/CBT (1/99) mixed SAM after fructose binding. For comparison, the SERS spectrum taken from the 4-MPBA/CBT (1/99) mixed SAM in PBS is also shown Figure 5. Several spectral changes are observed between the two spectra. The peak of 8a (1587 cm^{-1}), a totally symmetric mode, significantly decreased, while the peak of 8b (1574 cm^{-1}), a nontotally symmetric mode, increased. The peaks of the 19a (1487 cm^{-1}) and 19b (1472 cm^{-1}) modes varied in a similar trend. All these changes indicate that the symmetry of a 4-MPBA molecule is changed from nearly C_{2v} to C_s because of forming fructose-4-MPBA ester upon fructose binding.[40] The other changes of the peaks at

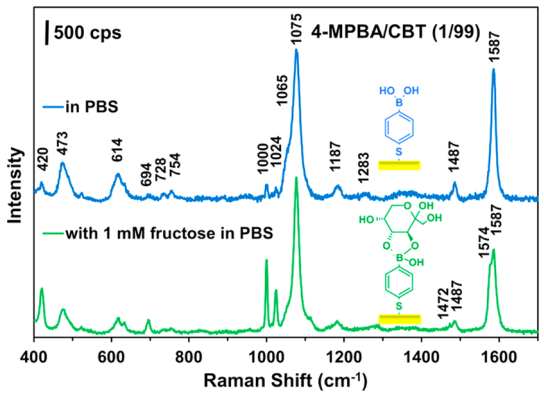

Figure 5. SERS spectra of 4-MPBA/CBT (1/99) mixed SAM on a Q3D-PNA in PBS (blue) and in PBS with 1 mM of fructose taken after 1 h of immersion (green). The inset illustration shows the symmetry breaking of 4-MPBA upon fructose binding. The λ_{ex} = 785 nm, P_{laser} = 1 mW, and t = 10 s.

420, 1000, 1024, and 1065 cm^{-1} related to the 7a + ν_{CS}, 12, 18a, and ν_{CS} modes, respectively, suggesting the possible reorientation and charge redistribution of the benzene ring. The results show that even with a very small amount of 4-MPBA molecules (5−6%) on the Q3D-PNA SERS substrate for the 4-MPBA/CBT (1/99) mixed SAM, the variation of the SERS spectrum of 4-MPBA upon fructose binding is still very obvious. Therefore, the 4-MPBA/CBT (1/99) mixed SAM modified Q3D-PNA SERS substrate exhibits both excellent nonfouling properties and capability to detect fructose.

Quantitative Detection of Fructose in PBS. Figure 6a shows the SERS spectra of the 4-MPBA/CBT (1/99) mixed SAM modified Q3D-PNA SERS substrates immersed in a series of concentrations of fructose from 0.01 to 1 mM, which is in the clinically relevant range.[41,42] The spectrum of each concentration was taken after immersion for 20 min to ensure quick, yet quantitative, measurement. Clearly, higher fructose concentration resulted in more obvious spectral changes. Figure 6a shows the Raman shift range of 950−1650 cm^{-1}, which contains the most distinct spectral changes. To completely extract and quantify the spectral information related to fructose concentrations, multivariate data analysis of PLS regression was applied for the evaluation. The PLS calibration model for fructose detection using the 4-MPBA/CBT (1/99) mixed SAM modified surfaces in PBS was obtained using spectra of 51 samples ranging from 0 to 1 mM. Each spectrum was preprocessed by normalizing the intensity to the 1075 cm^{-1} peak and then taking the Savitzky−Golay first derivative (5 points, second degree). The PLS factors were derived from the spectra from 950 to 1650 cm^{-1}. Figure 6b shows the first and second factors for PLS calibration. They are all related with the spectral changes of 4-MPBA upon fructose binding including the symmetry breaking and ring's reorientation. Figure 6c shows the root mean squared error of cross-validation (RMSECV) as a function of

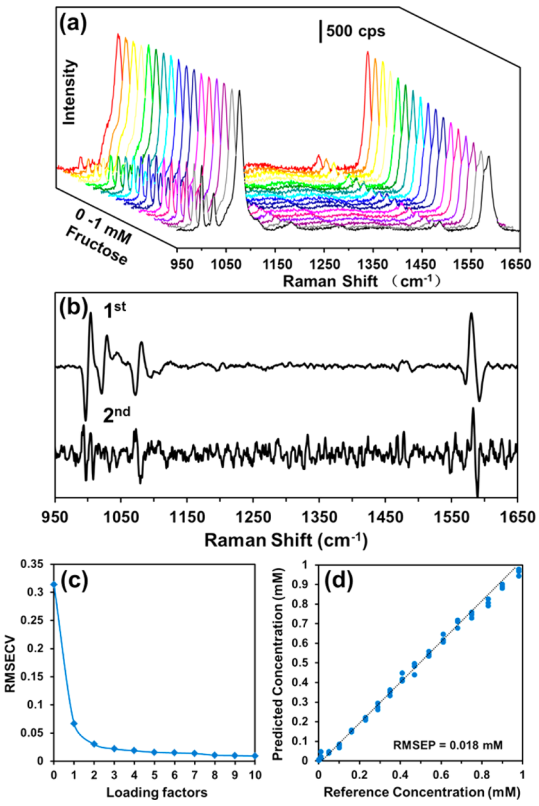

Figure 6. (a) SERS spectra of 4-MPBA/CBT (1/99) mixed SAM in fructose PBS solutions with the fructose concentrations of 0.01−1 mM after immersion for 20 min. The λ_{ex} = 785 nm, P_{laser} = 1 mW, and t = 10 s. (b) First two calibration factors used to produce PLS predictions. (c) The root mean squared error of cross-validation (RMSECV) as a function of number of loading factors used in the PLS algorithm. (d) Plot of PLS predicted fructose concentrations *versus* reference fructose concentrations using 4 loading factors.

loading factors, which indicates 4 loading factors work well to minimize the RMSECV, and meanwhile, describe the accuracy of the model itself. A satisfactory calibration was achieved using just four factors to avoid overmodeling data. Figure 6d shows the PLS result that a linear plot of predicted concentration *versus* actual concentration with R^2 = 0.99 generated by applying a leave-one-out cross-validated calibration model. The formal root mean squared error of prediction (RMSEP) is 0.018 mM, representing the accuracy of predicted concentration.

Accurate Fructose Detection in BSA Solution. To evaluate the accuracy of the fructose detection in BSA solution with the 4-MPBA/CBT (1/99) mixed SAM modified Q3D-PNA SERS substrates, we immersed the modified substrate in a 1 mg/mL BSA solution at 4 °C for 4 h and then the substrate was immersed in a 1 mg/mL BSA solution spiked with a series concentrations of fructose from 0.05 to 0.9 mM. The SERS spectra were taken after immersion for 20 min for each concentration and then to validate the predicted concentrations based on the PLS calibration model. The validation used 9 data points. The predicted concentrations were obtained

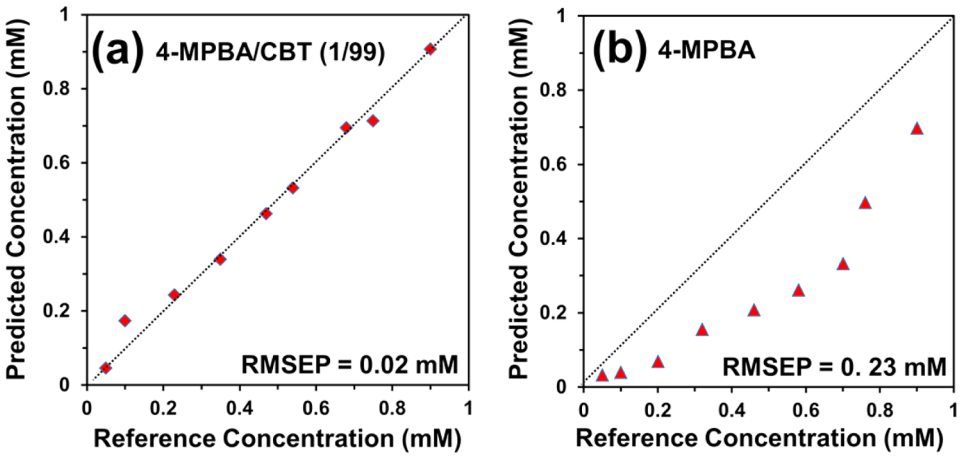

Figure 7. The plots of predicted fructose concentrations *versus* reference fructose concentrations on (a) 4-MPBA/CBT (1/99) mixed SAM and (b) pure 4-MPBA SAM modified SERS substrates, after immersion in the solution of 1 mg/mL BSA in PBS.

from the PLS calibration model built upon the results in PBS. Figure 7a shows the plot of the predicted concentrations *versus* the actual concentrations for the fructose detection in BSA solution after BSA blocking using the 4-MPBA/CBT (1/99) mixed SAM modified SERS substrate. Almost all the data points lie near the prefect prediction diagonal and the RMSEP is 0.02 mM. This result indicates that the 4-MPBA/CBT (1/99) mixed SAM modified Q3D-PNA SERS substrates maintain the detection accuracy and sensitivity as in PBS even after the substrates are immersed in BSA solution and the measurements are carried out at the presence of BSA in solution. This is because a 4-MPBA/CBT (1/99) mixed SAM highly resists protein fouling as demonstrated by the SPR measurement. In contrast, the detection accuracy is lost if the SERS substrates are modified by a pure 4-MPBA SAM. To quantitatively demonstrate this, we first built the PLS model for the pure 4-MPBA SAM modified surface using the SERS spectra of different concentrations of fructose in PBS as we did for the 4-MPBA/CBT (1/99) mixed SAM. We then took the SERS spectra of different concentrations of fructose in 1 mg/mL BSA solution after the BSA blocking as aforementioned. Figure 7b shows that all the predicted concentrations are smaller than the actual ones, with a RMSEP = 0.23 mM. Apparently, a protein fouling layer was formed on the pure 4-MPBA SAM modified SERS substrate during the blocking step as well as the subsequent detection step. The protein fouling layer inhibits the diffusion of fructose from the solution to the surface to bind with 4-MPBA and thereby suppresses the sensitivity and accuracy of the fructose detection.

CONCLUSIONS

In this work we demonstrated a stealth surface modification strategy for sensitive and accurate detection of fructose in protein solutions using SERS by modifying the SERS substrate with a mixed SAM of 4-MPBA and CBT. For the mixed SAM formed with a solution molar ratio of 1/99 of 4-MPBA and CBT, the surface exhibits excellent nonfouling properties with BSA adsorption around 3 ng/cm^2 measured by an SPR biosensor. Although the surface is occupied by approximately 94% of CBT for this mixed SAM, only 4-MPBA signals appear in the SERS spectrum because of the dramatic difference between their intrinsic Raman activities. The nonfouling property and invisibility in SERS spectra make CBT a stealth surface modification. The detections of fructose in protein solution over clinically relevant concentration range (0.01−1 mM) were carried out using the SERS substrates modified with this 4-MPBA/CBT (1/99) mixed SAM and a RMSEP of 0.018 mM was demonstrated by applying PLS regression analysis. The detection sensitivity and accuracy were maintained compared to the detections conducted in PBS. The concept of the stealth surface modification of SERS substrates could be adopted as a general strategy to introduce new functionalities to SERS substrates, while avoiding competition between the SERS signals of the target analyte and the surface modification.

MATERIALS AND METHODS

Materials. 4-Mercaptophenylboronic acid, D-(−)-fructose, phosphate buffered saline packet (PBS, pH 7.4 and ionic strength 150 mM) and albumin from bovine serum were purchased from Sigma-Aldrich (St. Louis, MO). Dithiothreitol, triethylamine, acrylic acid, and bis(2-dimethylaminoethyl) disulfide dihydrochloride were purchased from TCI America (Portland, OR). Diethyl ether and anhydrous methanol were purchased from J. T. Baker (Center Valley, PA). High-purity deionized (DI) water was obtained with a Millipore water purifier system.

Synthesis of *N,N*-Dimethyl-cysteamine-carboxybetaine. *N,N, N′,N′-Tetramethyl-cystamine-dicarboxybetaine (CBT Disulfide) (2).* Bis(2-dimethylaminoethyl) disulfide dihydrochloride **1** (10.1 g, 35.9 mmol) and triethylamine (10.0 mL, 71.7 mmol) were dissolved in

anhydrous methanol (100 mL) and the solution was stirred at room temperature for 30 min. Acrylic acid (48.3 mL, 710 mmol) and hydroquinone (500 mg, 4.54 mmol) were then added to the mixture, which was stirred at 50 °C for 18 h. The solution was concentrated on the rotovap to a syrupy consistency. Diethyl ether (500 mL) was added to the viscous residue resulting in a suspension that was stirred at room temperature for 12 h. The precipitate was filtered on a Buchner funnel, washed with cold ether and dried under high vacuum to afford the pure product as a fine white powder (11.6 g, 32.9 mmol). Yield: 92%. ^{1}H NMR (300 MHz, D_2O) δ (ppm): 3.60 (t, 4H, J = 7.6 Hz), 3.56 (t, 4H, J = 7.6 Hz), 3.07 (t, 4H, J = 4.7 Hz), 3.03 (s, 12H), 2.85 (t, 4H, J = 7.5 Hz).

N,N-Dimethyl-cysteamine-carboxybetaine (CBT) (3). CB-thiol disulfide **3** (3.20 g, 9.08 mmol) was dissolved in anhydrous methanol (50.0 mL). Dithiothreitol (1. 47 g, 9.53 mmol) was added to the solution and the mixture was stirred at room temperature for 12 h. The solution was concentrated on the rotovap to remove about 90% of methanol and diethyl ether (150 mL) was added to the residue, resulting in a suspension. After stirring in ether for 12 h, the precipitate was filtered out on a Buchner funnel, washed with ether and dried under high vacuum to afford the pure product as a white powder (1.37 g, 7.72 mmol). Yield: 85%. ^{1}H NMR (300 MHz, D_2O) δ (ppm): 3.51 (t, 2H, J = 6.4 Hz), 3.49 (t, 2H, J = 6.4 Hz), 2.97 (s, 6H), 2.82 (m, 4H). ^{13}C NMR (75 MHz, D_2O) δ (ppm): 174.4, 67.3, 60.8, 51.9, 29.1, 17.8.

Fabrication and Surface Modification of Gold Q3D-PNA SERS Substrates. Gold Q3D-PNA SERS substrates are composed of physically separated gold thin films with subwavelength nanoholes on the top and gold nanodiscs at the bottom of the wells as illustrated in Figure 1b. They were fabricated *via* electron beam lithography (EBL) following the same method reported previously.[25] Ellipsometery (J.A. Woollam, α-SE) was used to measure the thickness of PMMA and gold coatings, and the dimensions of the Q3D-PNA were confirmed by scanning electron microscope (SEM, FEI Sirion) shown in Figure 1c. Pure CBT, pure 4-MPBA, and 4-MPBA/CBT mixed SAMs were formed on the surface of a gold Q3D-PNA SERS substrates by soaking UV ozone-cleaned substrates in a 1 mM pure CBT, 1 mM pure 4-MPBA or 1 mM 4-MPBA/CBT (molar ratio: 10/90 and 1/99) absolute ethanol solution for 12 h, followed by rinsing with ethanol and deionized (DI) water and blowing dry in a stream of nitrogen.

Analysis of SAMs Using XPS. The pure CBT, pure 4-MPBA and 4-MPBA/CBT mixed SAMs were characterized using X-ray photoelectron spectroscopy (XPS) on a Kratos Axis Ultra XPS instrument using monochromated Al Kα radiation (1486.6 eV). Survey spectra and detail scans of C 1s, N 1s, B 1s, and S 2p were acquired using a pass energy of 150 eV. High-resolution spectra of C 1s and S 2p were acquired using a pass energy of 50 eV. Spectra were collected with the analyzer at 55° with respect to the surface normal of the sample. Typical pressure in the chamber during spectral acquisition was 10^{-9} Torr. Three spots on two or more replicates sample were analyzed. Computer aided surface analysis (CasaXPS) software was used to calculate compositions from the peak areas.

Nonfouling Assessment Using an SPR Biosensor. A four-channel custom-built SPR sensor was used to measure the protein adsorptions on the surfaces of gold SPR chips modified with different SAMs. The pure CBT, pure 4-MPBA and 4-MPBA/CBT mixed SAMs were formed on UV ozone-cleaned gold SPR chips following the same aforementioned method. The modified SPR chips were rinsed with ethanol, DI water, dried by nitrogen, and then mounted on the SPR device. The temperature controller was set to 25 ± 0.01 °C. Protein adsorption was measured by sequentially flowing PBS, 1 mg/mL BSA in PBS, and PBS over the SAM surface each for 10 min at 40 μL/min flow rate by a peristaltic pump. The wavelength shift between the baselines before protein injection and after rinsing with PBS was used to quantify the total amount of protein adsorbed. A reference channel containing a PBS flow was used for each chip to correct for baseline drift. A 1 nm wavelength shift from the SPR at 750 nm represents a surface coverage of 17 ng/cm^2 adsorbed proteins. The detection limit for the SPR sensor is 0.3 ng/cm^2.

Detection of Fructose in PBS and BSA Solutions Using SERS. A Renishaw InVia Raman spectroscope connected to a Leica DMLM upright microscope was used to collect SERS spectra. A 785 nm laser was used as an excitation laser, which was focused on a Q3D-PNA using a 50× (N.A. = 0.8) objective and the laser power of 1 mW. A spectral resolution of 1.1 cm^{-1} can be achieved, and spectra were collected in the range of 400−1700 cm^{-1}. The Q3D-PNA SERS substrates modified by pure CBT SAM, pure 4-MPBA SAM, or 4-MPBA/CBT mixed SAM were placed in a custom-made Teflon container, a volume of 150 μL PBS solution was added, and then a piece of microscope cover glass was placed on top of the container carefully to avoid forming bubbles. SERS spectra of 4-MPBA SAM and 4-MPBA/CBT mixed SAM were taken with CCD exposure time of 10 s and a single accumulation while those of CBT SAM with 10 accumulations to increase the signal/noise ratio. To detect fructose in PBS or proteins solutions, after placing a SERS substrate modified with 4-MPBA/CBT mixed SAM in the Teflon holder, a volume of 150 μL PBS solution or 1 mg/mL BSA solution spiked with concentrations of fructose (0.01, 0.05, 0.10, 0.16, 0.23, 0.29, 0.35, 0.41, 0.47, 0.54, 0.61, 0.68, 0.75, 0.83, 0.90, and 0.99 mM) was added on the surface carefully. Then the container was covered with a piece of microscope cover glass. The SERS spectra were collected after immersion in each concentration solution for 20 min with CCD exposure time of 10 s and a single accumulation. Three replicates were measured for each concentration.

Chemometrics Method. All SERS spectral data processing was performed using the Unscrambler X (CAMO Software, Oslo, Norway) software package.[43] Prior to analysis, all spectra were baseline corrected by fitting the raw spectrum to a fourth-order polynomial and then subtracted. The baseline corrected spectra were normalized with respect to the peak at 1075 cm^{-1} for 4-MPBA SAM and 4-MPBA/CBT SAM modified samples followed by taking the Savitzky−Golay first derivative (5 points, second degree). Then data analysis was conducted using partial least-squares (PLS) method with leave-one-out, cross validation for evaluating the effectiveness of SERS technique in predicting different fructose concentrations (0−1 mM) in PBS buffer.[44] This analysis used one sample as the validation set and the remaining samples as the training set. The process was repeated for all samples (*i.e.*, 51 samples). The root mean squared error of prediction (RMSEP) was used to judge the accuracy of predictions. It was calculated from the cross validation data as RMSEP = $[(1/51)\Sigma_{51}(\text{prediction} - \text{reference})^2]^{1/2}$.

For both of the pure 4-MPBA SAM and 4-MPBA/CBT mixed SAM modified SERS sensors, their PLS calibration models were built in PBS buffer. Then, the models were used for the prediction of different known concentrations of fructose in BSA solution after immersion of the modified sensors in BSA solution (1 mg/mL) for 4 h to evaluate the potential influence of protein fouling.

Conflict of Interest: The authors declare no competing financial interest.

Supporting Information Available: The assignments of SERS vibrational modes of 4-MPBA and CBT; high-resolution XPS spectra of the S 2p region of pure CBT SAM. This material is available free of charge *via* the Internet at http://pubs.acs.org.

Acknowledgment. This work was supported in part by National Science Foundation (NSF, CBET 1264470) and Defense Advanced Research Projects Agency (DARPA, N66001-12-1-4263) (S.J.) and NSF (CBET 1158609) (Q.Y.). EBL and Raman experiments were performed at the Nanotech User Facility (NTUF), the UW site of the National Nanotechnology Infrastructure Network (NNIN) supported by NSF.

Note Added after ASAP Publication: This paper was published ASAP on March 6, 2015. Scheme 1 and main text were updated. The revised paper was reposted on March 13, 2015.

REFERENCES AND NOTES

1. Schlucker, S. Surface-Enhanced Raman Spectroscopy: Concepts and Chemical Applications. *Angew. Chem., Int. Ed.* **2014**, *53*, 4756–4795.
2. Sharma, B.; Fernanda Cardinal, M.; Kleinman, S. L.; Greeneltch, N. G.; Frontiera, R. R.; Blaber, M. G.; Schatz, G. C.; Van Duyne, R. P. High-Performance SERS Substrates: Advances and Challenges. *MRS Bull.* **2013**, *38*, 615–624.

3. Vo-Dinh, T.; Wang, H. N.; Scaffidi, J. Plasmonic Nanoprobes for SERS Biosensing and Bioimaging. *J. Biophotonics* **2010**, *3*, 89–102.
4. Lindquist, N. C.; Nagpal, P.; McPeak, K. M.; Norris, D. J.; Oh, S. H. Engineering Metallic Nanostructures for Plasmonics and Nanophotonics. *Rep. Prog. Phys.* **2012**, 75.
5. Zhang, X. Y.; Young, M. A.; Lyandres, O.; Van Duyne, R. P. Rapid Detection of an Anthrax Biomarker by Surface-Enhanced Raman Spectroscopy. *J. Am. Chem. Soc.* **2005**, *127*, 4484–4489.
6. Aoki, P. H. B.; Furini, L. N.; Alessio, P.; Aliaga, A. E.; Constantino, C. J. L. Surface-Enhanced Raman Scattering (SERS) Applied to Cancer Diagnosis and Detection of Pesticides, Explosives, and Drugs. *Rev. Anal Chem.* **2013**, *32*, 55–76.
7. Cao, Y. W. C.; Jin, R. C.; Mirkin, C. A. Nanoparticles with Raman Spectroscopic Fingerprints for DNA and RNA Detection. *Science* **2002**, *297*, 1536–1540.
8. Graham, D.; Faulds, K. Quantitative SERRS for DNA Sequence Analysis. *Chem. Soc. Rev.* **2008**, *37*, 1042–1051.
9. Barhoumi, A.; Zhang, D.; Tam, F.; Halas, N. J. Surface-Enhanced Raman Spectroscopy of DNA. *J. Am. Chem. Soc.* **2008**, *130*, 5523–5529.
10. Han, X. X.; Zhao, B.; Ozaki, Y. Surface-Enhanced Raman Scattering for Protein Detection. *Anal Bioanal Chem.* **2009**, *394*, 1719–1727.
11. Xu, J. J.; Zhang, L.; Gong, H.; Homola, J.; Yu, Q. M. Tailoring Plasmonic Nanostructures for Optimal SERS Sensing of Small Molecules and Large Microorganisms. *Small* **2011**, *7*, 371–376.
12. Jarvis, R. M.; Goodacre, R. Characterisation and Identification of Bacteria Using SERS. *Chem. Soc. Rev.* **2008**, *37*, 931–936.
13. Xu, J. J.; Turner, J. W.; Idso, M.; Biryukov, S. V.; Rognstad, L.; Gong, H.; Trainer, V. L.; Wells, M. L.; Strom, M. S.; Yu, Q. M. *In Situ* Strain-Level Detection and Identification of *Vibrio parahaemolyticus* Using Surface-Enhanced Raman Spectroscopy. *Anal. Chem.* **2013**, *85*, 2630–2637.
14. Vendrell, M.; Maiti, K. K.; Dhaliwal, K.; Chang, Y. T. Surface-Enhanced Raman Scattering in Cancer Detection and Imaging. *Trends Biotechnol.* **2013**, *31*, 249–257.
15. Bantz, K. C.; Meyer, A. F.; Wittenberg, N. J.; Im, H.; Kurtulus, O.; Lee, S. H.; Lindquist, N. C.; Oh, S. H.; Haynes, C. L. Recent Progress in SERS Biosensing. *Phys. Chem. Chem. Phys.* **2011**, *13*, 11551–11567.
16. Lyandres, O.; Shah, N. C.; Yonzon, C. R.; Walsh, J. T.; Glucksberg, M. R.; Van Duyne, R. P. Real-Time Glucose Sensing by Surface-Enhanced Raman Spectroscopy in Bovine Plasma Facilitated by a Mixed Decanethiol/Mercaptohexanol Partition Layer. *Anal. Chem.* **2005**, *77*, 6134–6139.
17. Stewart, A.; Bell, S. E. J. Modification of Ag Nanoparticles with Mixed Thiols for Improved SERS Detection of Poorly Adsorbing Target Molecules: Detection of MDMA. *Chem. Commun.* **2011**, *47*, 4523–4525.
18. Yang, J.; Palla, M.; Bosco, F. G.; Rindzevicius, T.; Alstrom, T. S.; Schmidt, M. S.; Boisen, A.; Ju, J. Y.; Lin, Q. Surface-Enhanced Raman Spectroscopy Based Quantitative Bioassay on Aptamer-Functionalized Nanopillars Using Large-Area Raman Mapping. *ACS Nano* **2013**, *7*, 5350–5359.
19. He, L. L.; Lamont, E.; Veeregowda, B.; Sreevatsan, S.; Haynes, C. L.; Diez-Gonzalez, F.; Labuza, T. P. Aptamer-Based Surface-Enhanced Raman Scattering Detection of Ricin in Liquid Foods. *Chem. Sci.* **2011**, *2*, 1579–1582.
20. Kho, K. W.; Dinish, U. S.; Kumar, A.; Olivo, M. Frequency Shifts in SERS for Biosensing. *ACS Nano* **2012**, *6*, 4892–4902.
21. Guarrotxena, N.; Bazan, G. C. Antitags: SERS-Encoded Nanoparticle Assemblies that Enable Single-Spot Multiplex Protein Detection. *Adv. Mater.* **2014**, *26*, 1941–1946.
22. Pallaoro, A.; Braun, G. B.; Reich, N. O.; Moskovits, M. Mapping Local pH in Live Cells Using Encapsulated Fluorescent SERS Nanotags. *Small* **2010**, *6*, 618–622.
23. Kneipp, J.; Kneipp, H.; Wittig, B.; Kneipp, K. One- and Two-Photon Excited Optical pH Probing for Cells Using Surface-Enhanced Raman and Hyper-Raman Nanosensors. *Nano Lett.* **2007**, *7*, 2819–2823.
24. Guerrini, L.; Pazos, E.; Penas, C.; Vazquez, M. E.; Mascarenas, J. L.; Alvarez-Puebla, R. A. Highly Sensitive SERS Quantification of the Oncogenic Protein c-Jun in Cellular Extracts. *J. Am. Chem. Soc.* **2013**, *135*, 10314–10317.
25. Sun, F.; Bai, T.; Zhang, L.; Ella-Menye, J. R.; Liu, S. J.; Nowinski, A. K.; Jiang, S. Y.; Yu, Q. M. Sensitive and Fast Detection of Fructose in Complex Media *via* Symmetry Breaking and Signal Amplification Using Surface-Enhanced Raman Spectroscopy. *Anal. Chem.* **2014**, *86*, 2387–2394.
26. Zayak, A. T.; Hu, Y. S.; Choo, H.; Bokor, J.; Cabrini, S.; Schuck, P. J.; Neaton, J. B. Chemical Raman Enhancement of Organic Adsorbates on Metal Surfaces. *Phys. Rev. Lett.* **2011**, 106.
27. Wang, F. L.; Widejko, R. G.; Yang, Z. Q.; Nguyen, K. T.; Chen, H. Y.; Fernando, L. P.; Christensen, K. A.; Anker, J. N. Surface-Enhanced Raman Scattering Detection of pH with Silica-Encapsulated 4-Mercaptobenzoic Acid-Functionalized Silver Nanoparticles. *Anal. Chem.* **2012**, *84*, 8013–8019.
28. Larmour, I. A.; Graham, D. Surface Enhanced Optical Spectroscopies for Bioanalysis. *Analyst* **2011**, *136*, 3831–3853.
29. Holmlin, R. E.; Chen, X. X.; Chapman, R. G.; Takayama, S.; Whitesides, G. M. Zwitterionic SAMs that Resist Nonspecific Adsorption of Protein from Aqueous Buffer. *Langmuir* **2001**, *17*, 2841–2850.
30. Chen, S. F.; Zheng, J.; Li, L. Y.; Jiang, S. Y. Strong Resistance of Phosphorylcholine Self-Assembled Monolayers to Protein Adsorption: Insights into Nonfouling Properties of Zwitterionic Materials. *J. Am. Chem. Soc.* **2005**, *127*, 14473–14478.
31. Alvarez-Puebla, R. A.; Aroca, R. F. Synthesis of Silver Nanoparticles with Controllable Surface Charge and Their Application to Surface-Enhanced Raman Scattering. *Anal. Chem.* **2009**, *81*, 2280–2285.
32. Socrates, G. *Infrared and Raman Characteristic Group Frequencies: Tables and Charts*; John Wiley & Sons: New York, 2004; pp 107−125.
33. Pigorsch, E. Spectroscopic Characterisation of Cationic Quaternary Ammonium Starches. *Starch/Staerke* **2009**, *61*, 129–138.
34. Graff, M.; Bukowska, J. Adsorption of Enantiomeric and Racemic Cysteine on a Silver Electrode—SERS Sensitivity to Chirality of Adsorbed Molecules. *J. Phys. Chem. B* **2005**, *109*, 9567–9574.
35. Szafranski, C. A.; Tanner, W.; Laibinis, P. E.; Garrell, R. L. Surface-Enhanced Raman Spectroscopy of Aromatic Thiols and Disulfides on Gold Electrodes. *Langmuir* **1998**, *14*, 3570–3579.
36. Fu, M. D.; Chen, W. P.; Lu, H. C.; Kuo, C. T.; Tseng, W. H.; Chen, C. H. Conductance of Alkanediisothiocyanates: Effect of Headgroup-Electrode Contacts. *J. Phys. Chem. C* **2007**, *111*, 11450–11455.
37. Han, S. W.; Lee, S. J.; Kim, K. Self-Assembled Monolayers of Aromatic Thiol and Selenol on Silver: Comparative Study of Adsorptivity and Stability. *Langmuir* **2001**, *17*, 6981–6987.
38. Briggs, D. *Surface Analysis of Polymers by XPS and Static SIMS*; Cambridge University Press: Cambridge, U.K., 1998; pp 65−69.
39. Barriet, D.; Yam, C. M.; Shmakova, O. E.; Jamison, A. C.; Lee, T. R. 4-Mercaptophenylboronic Acid SAMs on Gold: Comparison with SAMs Derived from Thiophenol, 4-Mercaptophenol, and 4-Mereaptobenzoic Acid. *Langmuir* **2007**, *23*, 8866–8875.
40. Centeno, S. P.; Lopez-Tocon, I.; Roman-Perez, J.; Arenas, J. F.; Soto, J.; Otero, J. C. Franck-Condon Dominates the Surface-Enhanced Raman Scattering of 3-Methylpyridine: Propensity Rules of the Charge-Transfer Mechanism under Reduced Symmetry. *J. Phys. Chem. C* **2012**, *116*, 23639–23645.
41. Tasevska, N.; Runswick, S. A.; McTaggart, A.; Bingham, S. A. Urinary Sucrose and Fructose as Biomarkers for Sugar Consumption. *Cancer Epidemiol., Biomarkers Prev.* **2005**, *14*, 1287–1294.
42. Kawasaki, T.; Akanuma, H.; Yamanouchi, T. Y. Increased Fructose Concentrations in Blood and Urine in Patients with Diabetes. *Diabetes Care* **2002**, *25*, 353–357.
43. Chretien, J. R. The Unscrambler, the Software in Chemometrics - Version 7.0 from CAMO Company, Oslo, Norway. *Analusis* **1998**, *26*, M11–M12.
44. Martens, H. *Multivariate Calibration*; John Wiley & Sons: New York, 1989; pp 116−163.